Electronic Supplementary Material (ESI) for Journal of Materials Chemistry A.

Supporting Information

Linker engineering to regulate fluorescence of hydrazone-linked covalent organic frameworks for real-time visual detection of norfloxacin and multiple information encryption

Haifei Wan, Mengyao Li, Li Wang* and Yonghai Song*

College of Chemistry and Chemical Engineering, Jiangxi Normal University, 99 Ziyang Avenue, Nanchang 330022, China.

∗Corresponding author: Tel/Fax: +86 791 88120861. E-mail: lwang@jxnu.edu.cn (L. Wang), yhsonggroup@hotmail.com or yhsong@jxnu.edu.cn (Y. Song).

Experimental

Reagent. 2, 5-bis(2-methoxyethoxy)p-phenyldiphenylhydrazine (TFPB), benzaldehyde (TFB), 1,3, 5-trimethoxy-2,4, 6-triformylbenzene (TB), 2,4, 6-triformylhomecoglucinol (TBT), and 2-hydroxy-1,3, 5-benzaldehyde (HB) were purchased from Jilin Yanshen Technology Co., Ltd. of the Chinese Academy of Sciences (Changchun, China). Solvents including mesitylene, N, N-dimethylacetamide (DMF), N, N-dimethyl acetamide (DMA)，dimethyl sulfoxide (DMSO), tetrahydrofuran (THF), methanol, ethanol and others were purchased from Xilong Chemical Co., Ltd (Guangzhou, China). Acetic acid and 1,4-dioxane were purchased from Shanghai Aladdin Reagent Co., Ltd (Shanghai, China). Norfloxacin (NOR), pyrogallic acid (PA), dimethidazole (DT), amoxicillin (AMX), Flufenicol (FF), Ribavirin (RBV), sulfamethoxylacil (SO), metringamycin (MG), Aprovir (AW), Furfurone hydrochloride (FH), Albendazole (ABZ), furantoin (AHD) were purchased from Pedder Medical Technology Co., LTD. (Shanghai, China). All reagents are analytically pure and do not need to be purified again.

Instruments. The excitation and emission spectra of 2,5-bis(2-methoxyethoxy-p-phenylhydrazine) -based COFs in a solution were detected on Hitachi F-7000 fluorescence spectrophotometer. The emission spectra of solid-state 2,5-bis(2-methoxyethoxy-p-phenylhydrazine)-based COFs were detected on Edinburgh FLS980 fluorescence spectrophotometer. The solid-state UV-vis absorption spectra were recorded by Shimadzu UV-3600i ultraviolet spectrophotometer. Scanning electron microscopy (SEM) was employed using HITACHIS-3400N (Hitachi, Japan) with an acceleration voltage of 15 KV. Fourier transform infrared spectroscopy (FTIR) was measured by Perkin-Elmer's 200 spectrometer. On the D/Max 2500 V/PC X-ray powder diffractometer, X-ray diffraction (XRD) data was collected with Cu K Kα radiation (λ=1.54056 Å, 40 kV, 200 mA). N_2 adsorption/desorption

isotherm tests were carried out by Autosorb-iQ (Quantachrome, USA) under 77 K. Thermogravimetric analysis (TGA) was performed by TG6300 at a temperature of 10 °C min^{-1} in a nitrogen atmosphere.

Fluorescence measurements. The powder of 1.0 mg finely grounded $COF_{BMTH-TFB}$, $COF_{BMTH-TB}$, $COF_{BMTH-TBT}$ and $COF_{BMTH-HB}$ were dissolved in 1 mL solvents (DMA, DMF, DMSO, H_2O, THF, Acetone, Methanol, Ethanol) and sonicated until complete dissolution to prepare the concentration of 1 mg L^{-1} $COF_{BMTH-TFB}$, $COF_{BMTH-TB}$, $COF_{BMTH-TBT}$ and $COF_{BMTH-HB}$ solution. The fluorescence properties of the materials were investigated at room temperature. The concentration of NOR was determined by fluorescence titration. The emission spectra were monitored at the excitation wavelength of 370 nm. Then the intensity of emission peak at 450 nm was analyzed. Interference experiments and selectivity tests were performed in the above method by replacing NOR with other interfering substances, the concentration of interfering substances was 100 μg mL^{-1} in the probe solution, and the concentration of NOR added was 20 μg mL^{-1}.

DFT calculation. The geometric structures of $COF_{BMTH-TFB}$, $COF_{BMTH-TB}$, $COF_{BMTH-TBT}$ and $COF_{BMTH-HB}$ in ground and excited states and the frontier molecular orbitals were calculated by using DFT method, CAM-B3LYP functional and 6-31G(d) basis set. The Gaussian09 software package was used for calculation.

Preparation of fluorescent test paper. First, the filter paper was cut into round pieces with a diameter of 0.5 cm. Then the round pieces were immersed in $COF_{BMTH-TFB}$, $COF_{BMTH-TB}$, $COF_{BMTH-TBT}$ and $COF_{BMTH-HB}$ solution for 6 h with concentrations of 1 mg mL^{-1}, 2 mg mL^{-1}, 2 mg mL^{-1} and 2 mg mL^{-1}, respectively. Subsequently, the round pieces were taken out and laid in a petri dish and dried at room temperature for subsequent experiments.

Smart phone APP recognition and RGB intelligent analysis. The "ColorColl" APP in smart phone

was used for RBG analysis of color changes in the process of NOR detection. The APP can read the colors and convert them to R, G, and B values (R= red, G= green, B= blue).

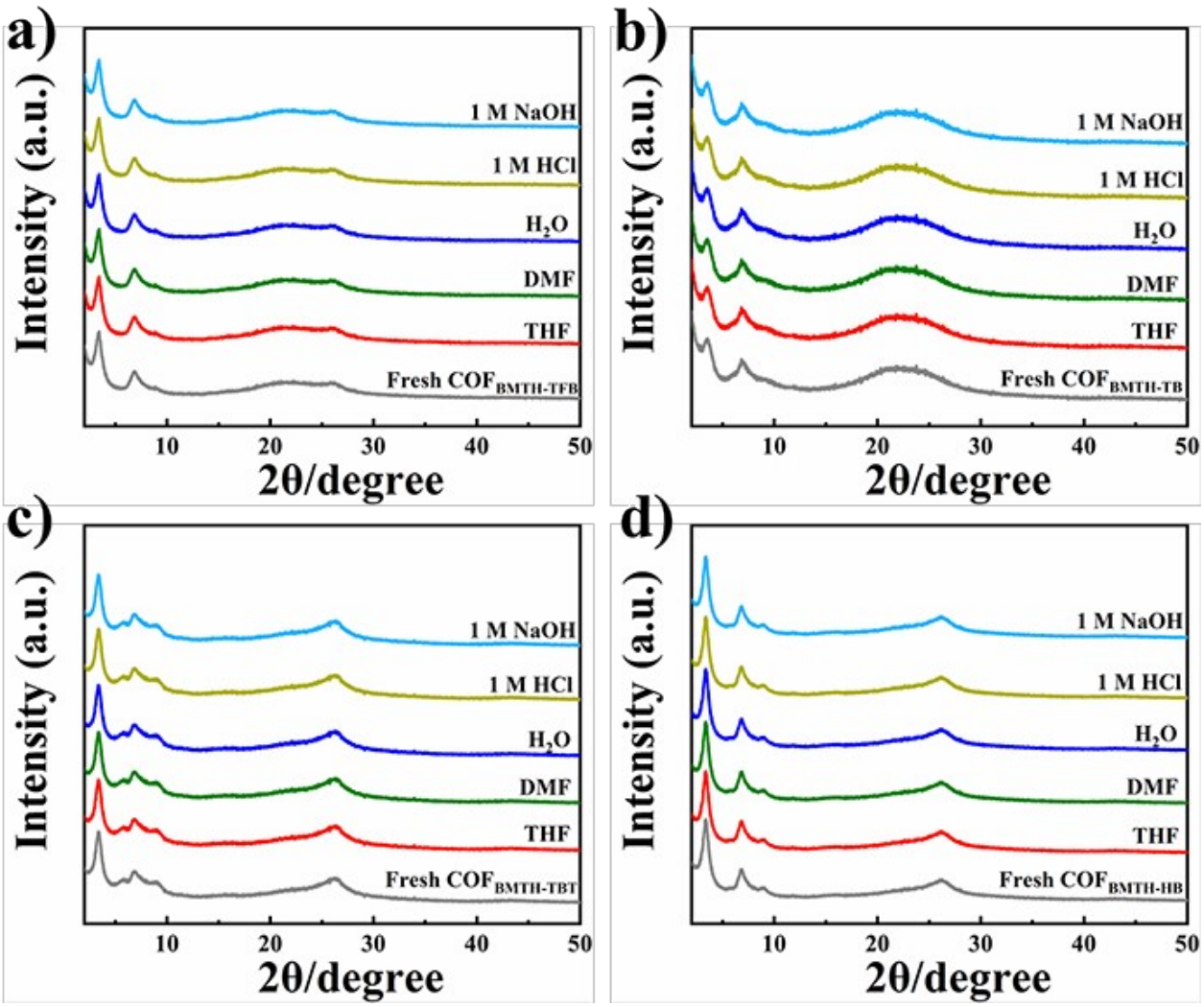

Fig. S1. The PXRD patterns of $COF_{BMTH\text{-}TFB}$ (a), $COF_{BMTH\text{-}TB}$ (b), $COF_{BMTH\text{-}TBT}$ (c) and $COF_{BMTH\text{-}HB}$ (d) immersed in various solvents for 12 h, including THF, DMF, H_2O, HCl (1 M) and NaOH (1 M) solution.

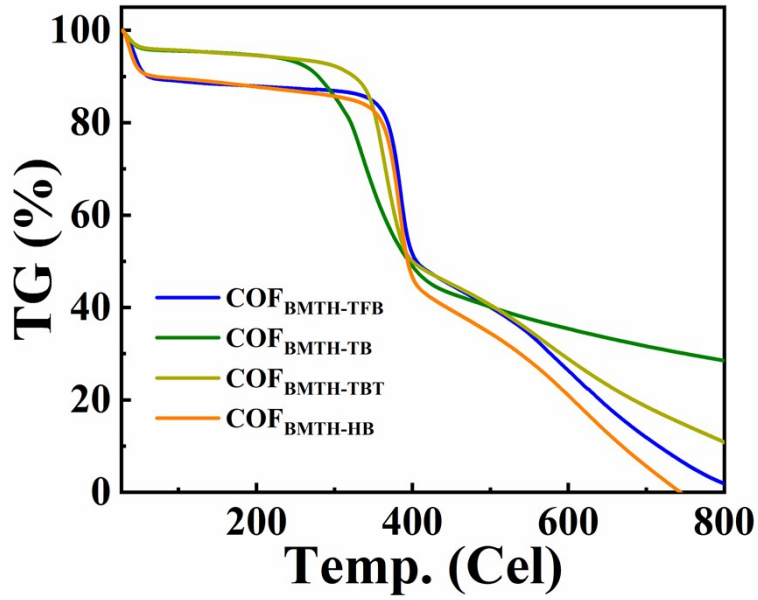

Fig. S2. TGA curves for $COF_{BMTH\text{-}TFB}$, $COF_{BMTH\text{-}TB}$, $COF_{BMTH\text{-}TBT}$ and $COF_{BMTH\text{-}HB}$.

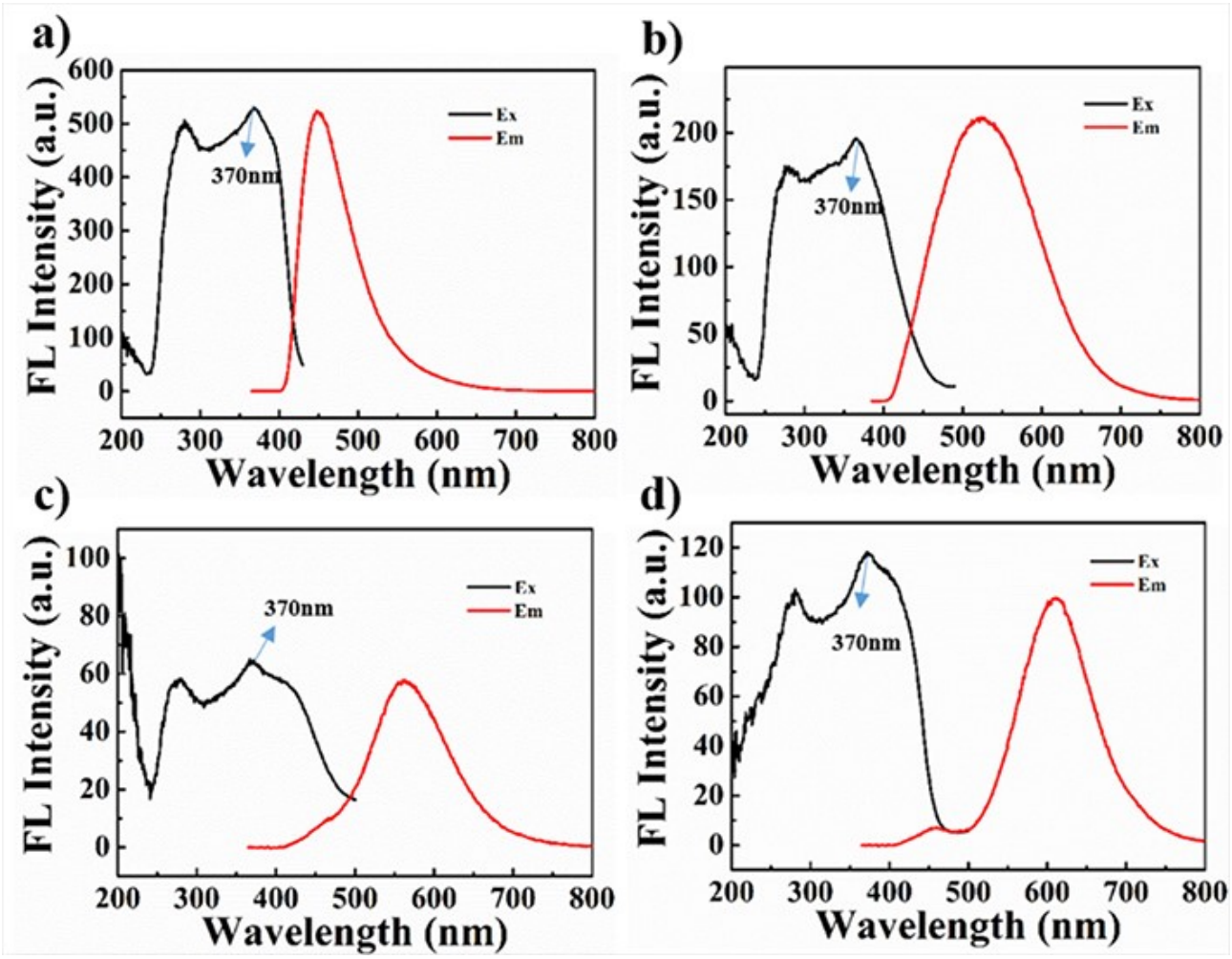

Fig. S3. Excitation and emission spectra of $COF_{BMTH\text{-}TFB}$ (a), $COF_{BMTH\text{-}TB}$ (b), $COF_{BMTH\text{-}TBT}$ (c) and $COF_{BMTH\text{-}HB}$ (d).

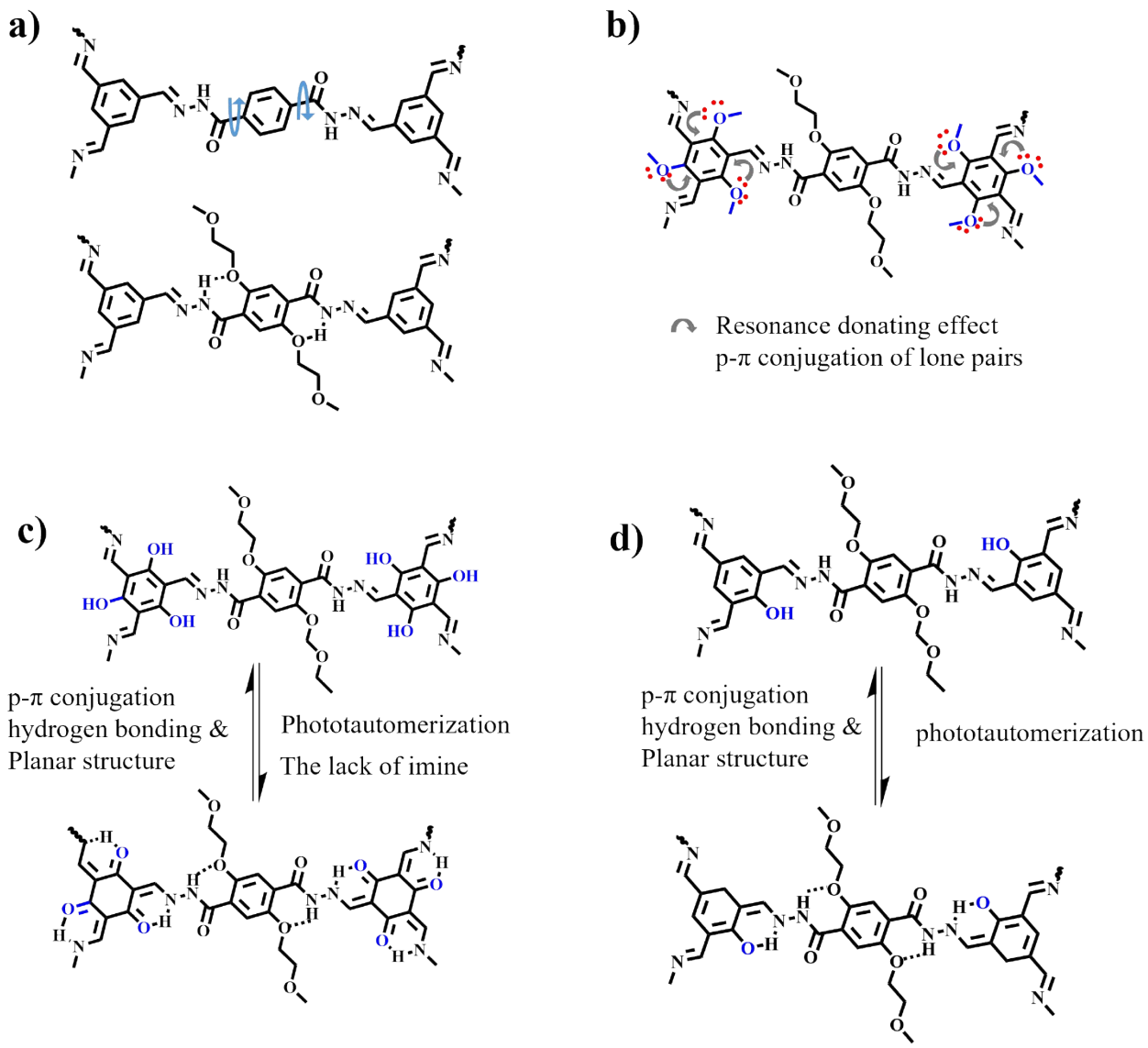

Fig. S4. The luminescence mechanisms of $COF_{BMTH\text{-}TFB}$ (a), $COF_{BMTH\text{-}TB}$ (b), $COF_{BMTH\text{-}TBT}$ (c) and $COF_{BMTH\text{-}HB}$ (d).

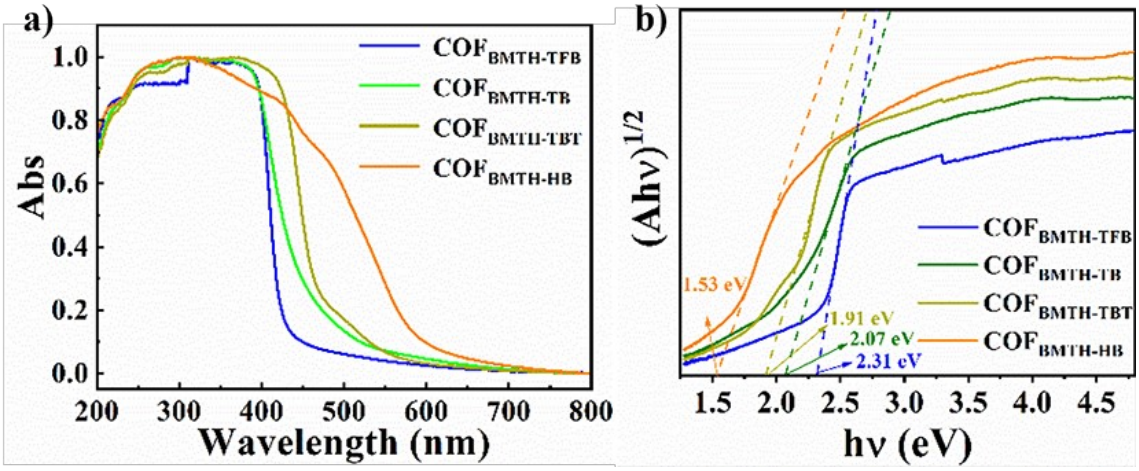

Fig. S5. (a) UV-vis absorption spectra and (b) Kubelka-Munk plots of $COF_{BMTH\text{-}TFB}$, $COF_{BMTH\text{-}TB}$, $COF_{BMTH\text{-}TBT}$ and $COF_{BMTH\text{-}HB}$, respectively.

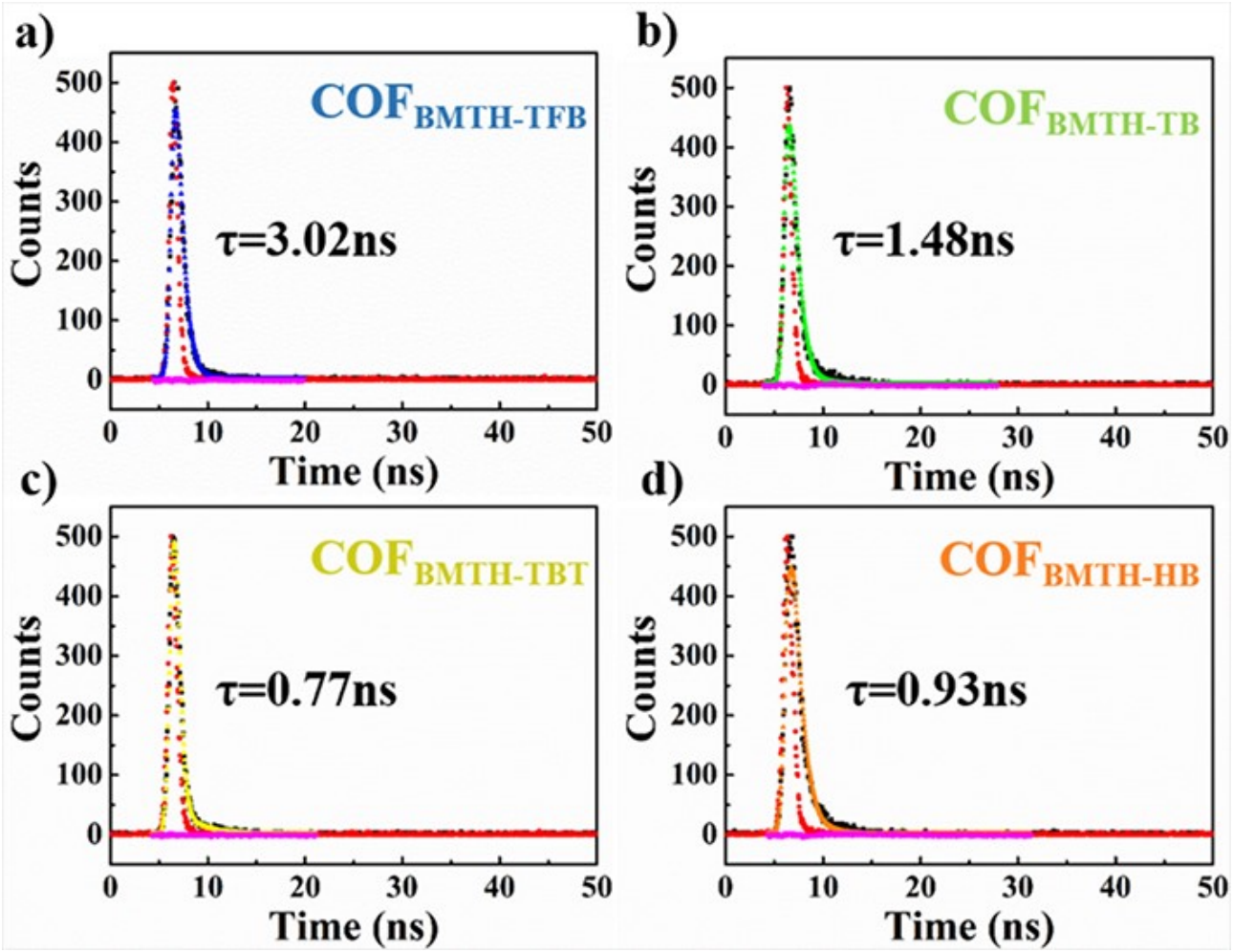

Fig. S6. Fluorescence lifetime plots of (a) $COF_{BMTH\text{-}TFB}$, (b) $COF_{BMTH\text{-}TB}$, (c) $COF_{BMTH\text{-}TBT}$ and (d) $COF_{BMTH\text{-}HB}$.

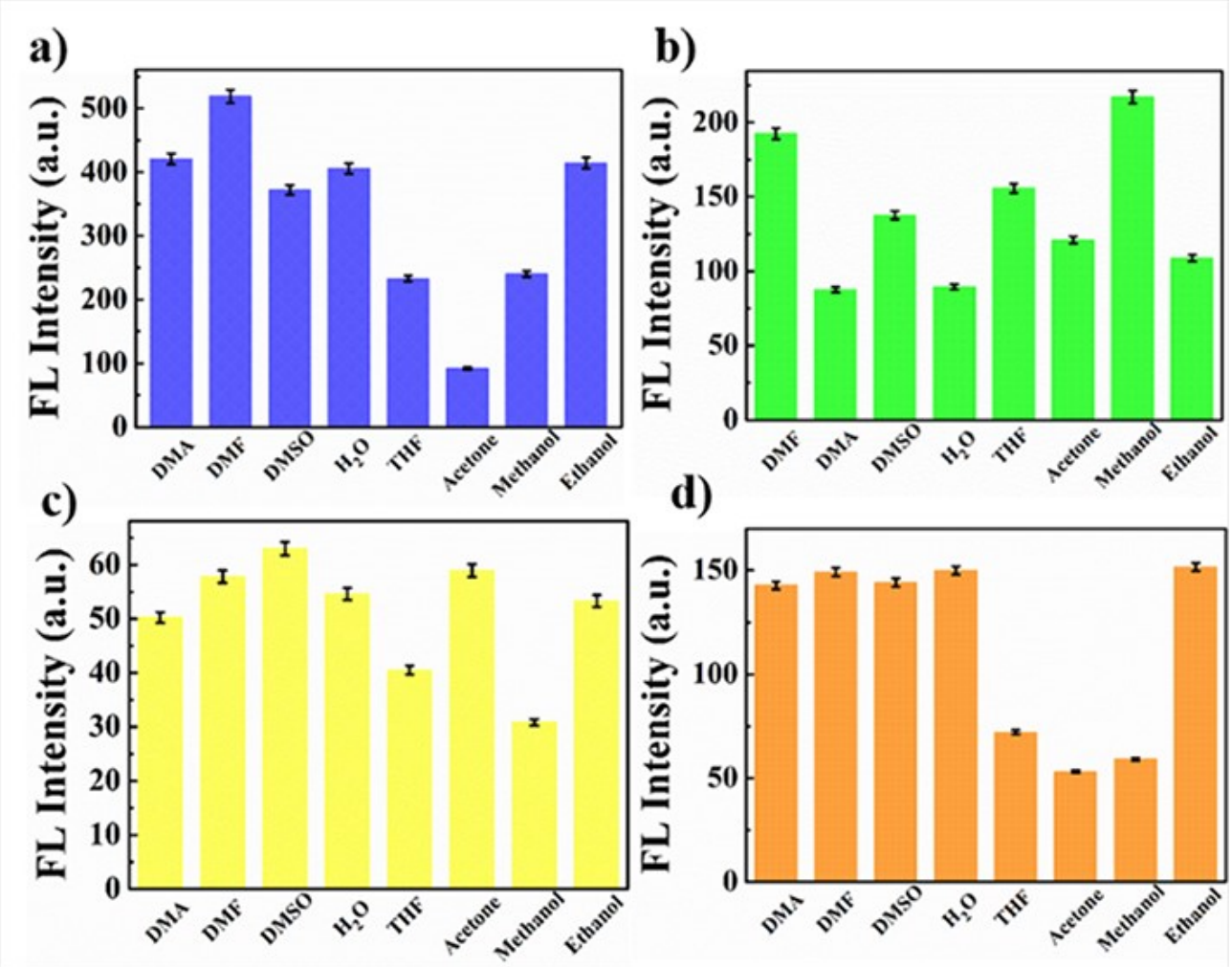

Fig. S7. Histogram of fluorescence emission intensity of (a) $COF_{BMTH\text{-}TFB}$, (b) $COF_{BMTH\text{-}TB}$, (c) $COF_{BMTH\text{-}TBT}$ and (d) $COF_{BMTH\text{-}HB}$ in different solvents.

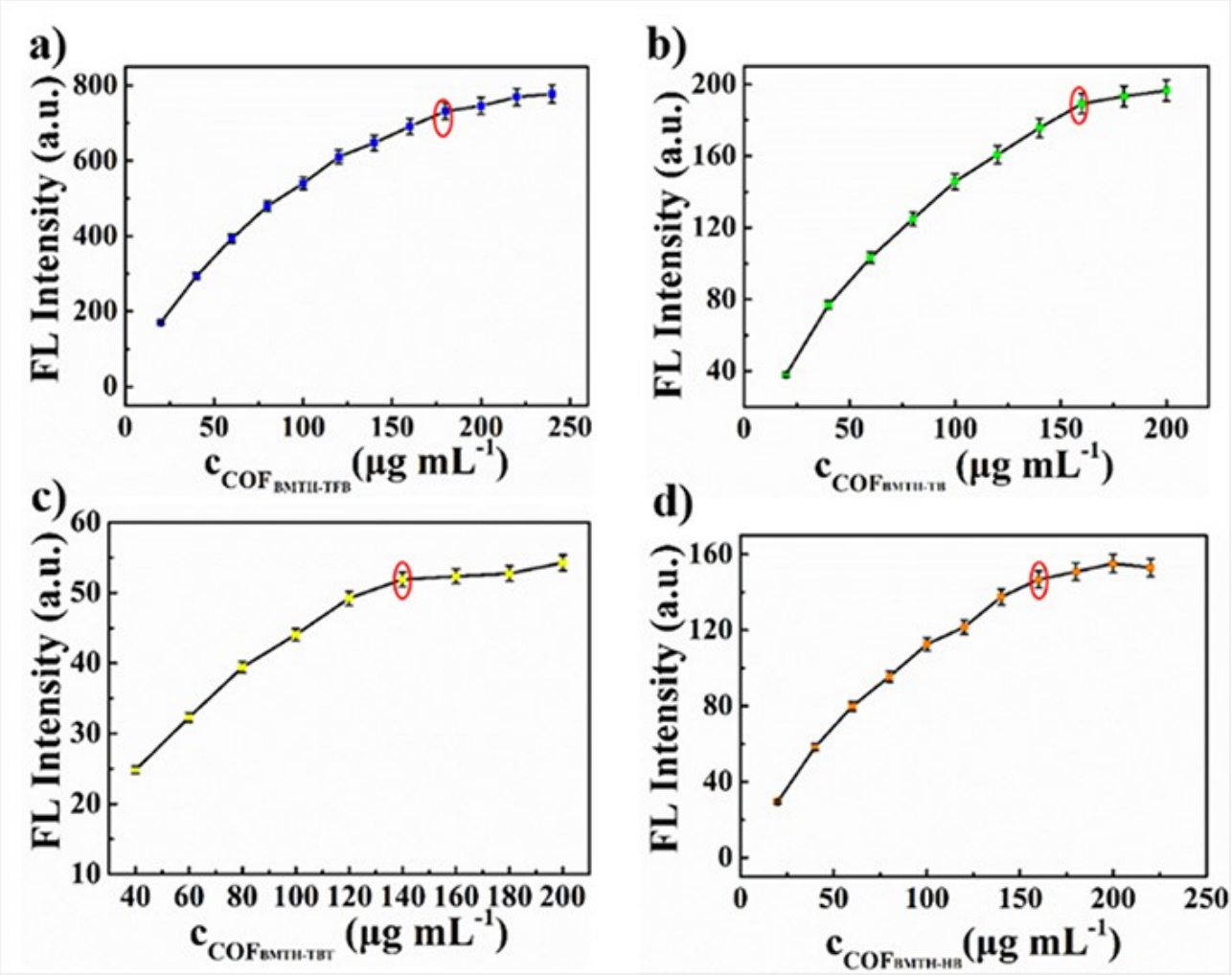

Fig. S8. Fluorescence emission intensity curves of (a) $COF_{BMTH-TFB}$, (b) $COF_{BMTH-TB}$, (c) $COF_{BMTH-TBT}$ and (d) $COF_{BMTH-HB}$ at different concentrations.

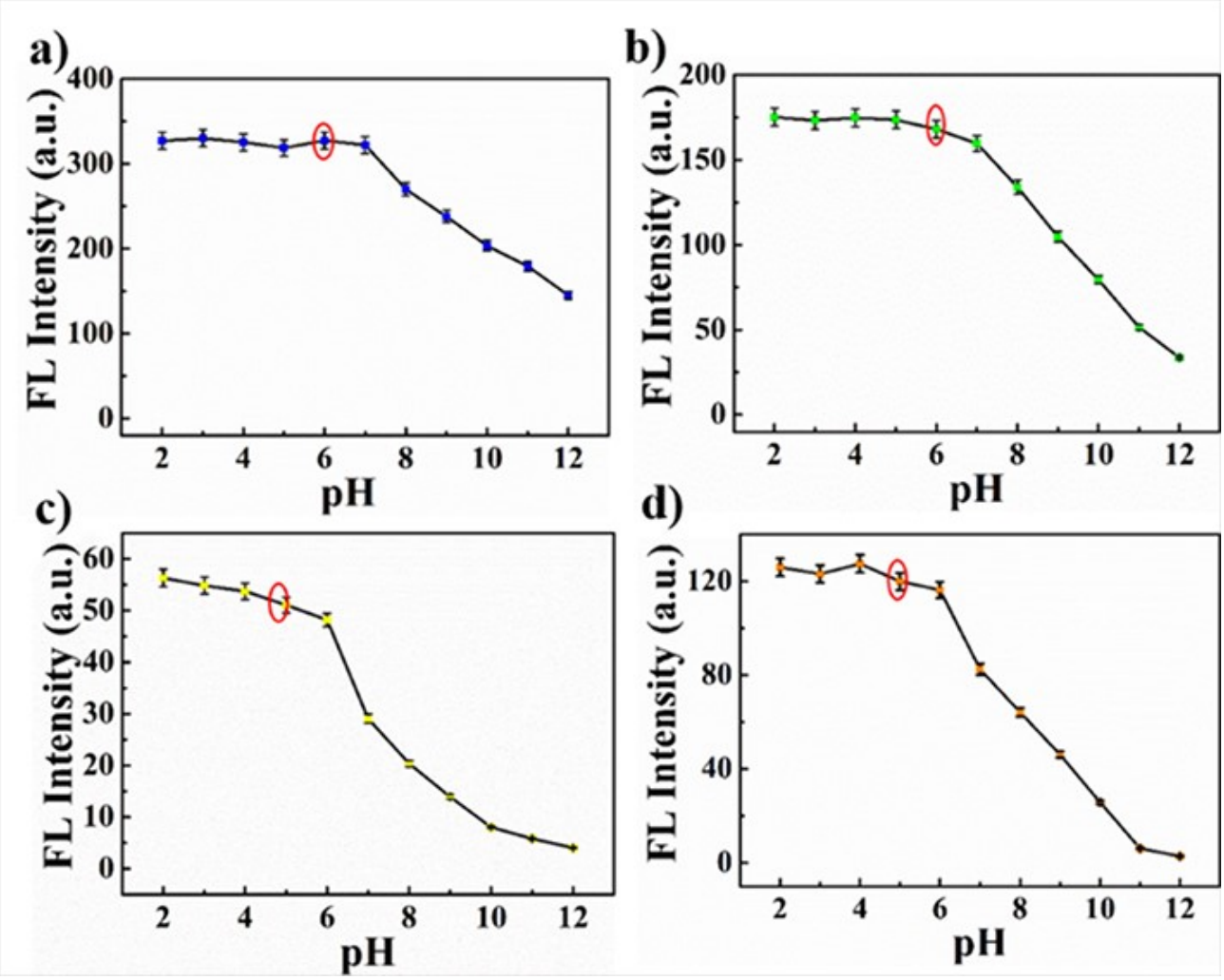

Fig. S9. Fluorescence emission intensity curves of (a) $COF_{BMTH\text{-}TFB}$, (b) $COF_{BMTH\text{-}TB}$, (c) $COF_{BMTH\text{-}TBT}$ and (d) $COF_{BMTH\text{-}HB}$ at different pH.

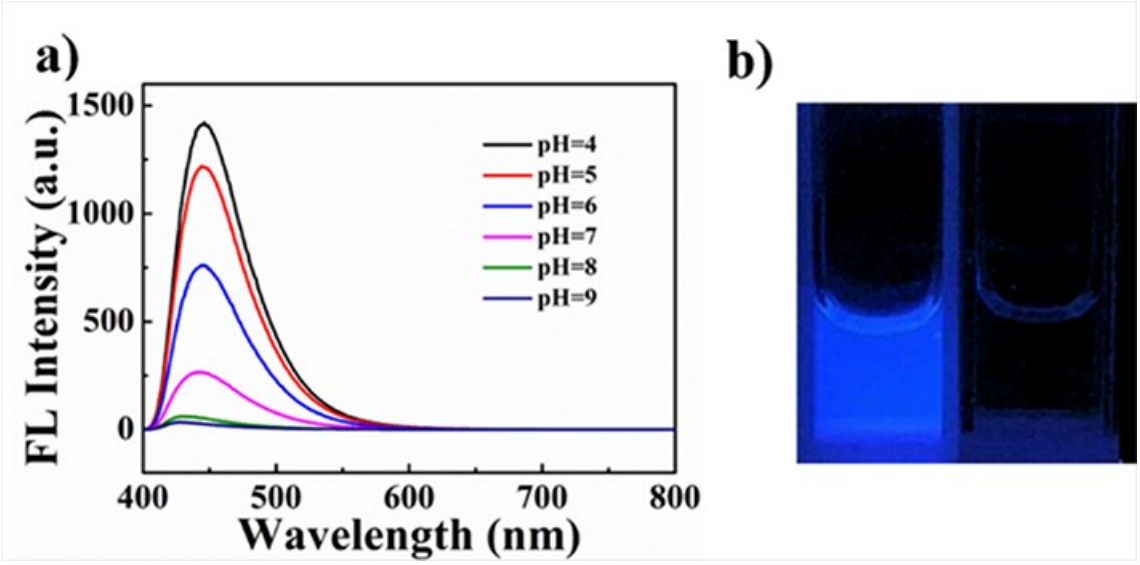

Fig. S10. (a) Fluorescence emission spectra of NOR with the same concentration in PBS with different pH. (b) Photographs of NOR at the same concentration in PBS (pH=6) (left) and water (right) under 365 nm UV lamp.

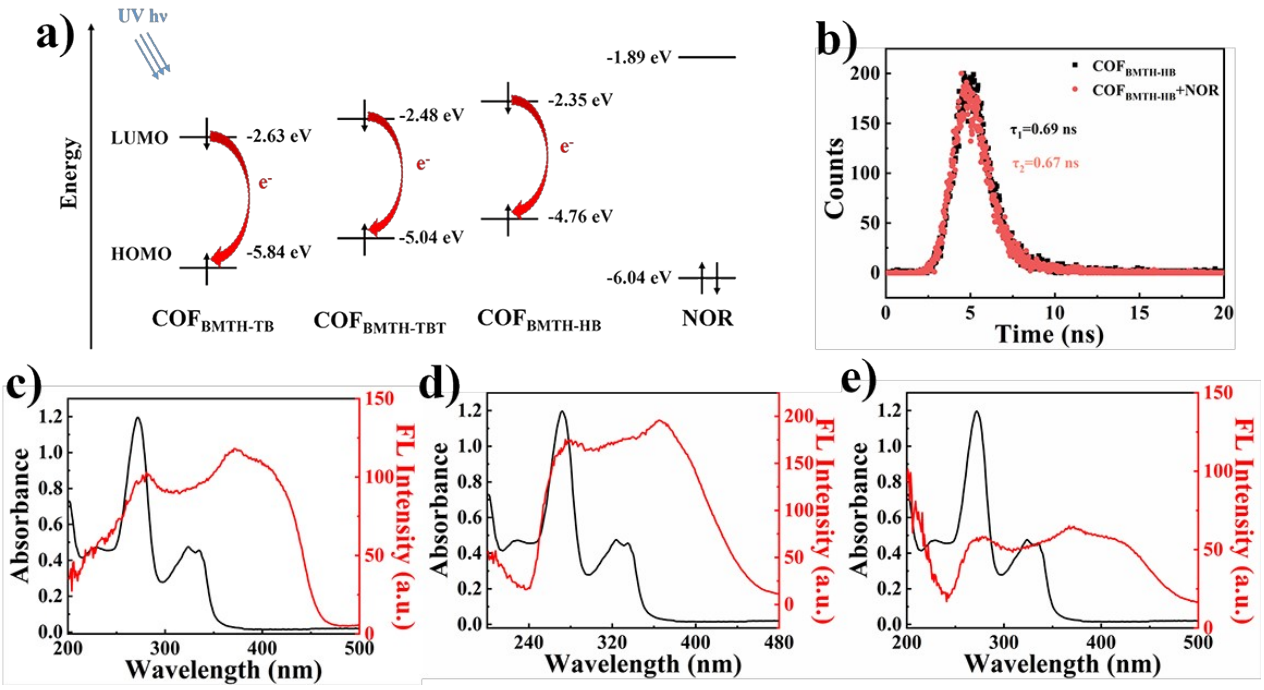

Fig. S11. (a) HOMO and LUMO energies for $COF_{BMTH-TB}$, $COF_{BMTH-TBT}$, $COF_{BMTH-HB}$ and NOR. (b) The fluorescence lifetime of $COF_{BMTH-HB}$ before and after the addition of NOR. Uv-vis absorption spectra of NOR (black line) and excitation spectra of $COF_{BMTH-HB}$ (red line) (c), $COF_{BMTH-TB}$(d) and $COF_{BMTH-TBT}$ (e).

In order to further understand the fluorescence quenching effect of NOR on $COF_{BMTH-HB}$, the possible mechanism of fluorescence quenching was systematically studied. In order to investigate whether fluorescence quenching originates from the photoinduced electron transfer (PET), HOMO and LUMO energy levels of NOR were calculated using DFT. It was found that the HOMO level of NOR was lower than the HOMO level of $COF_{BMTH-HB}$, and the LUMO level of NOR was higher than the LUMO level of $COF_{BMTH-HB}$ (Fig. S11a). The electrons in the excited state of $COF_{BMTH-HB}$ can return to the ground state normally. Therefore, the PET mechanism can be excluded. Then, the fluorescence lifetimes of COF before and after the addition of NOR were calculated by time-resolved fluorescence, and measured to be 0.69 and 0.67 ns, respectively, which were essentially unchanged (Fig. S11b). The quenching mechanism of COF was further determined by using the Stern-Volmer equation, and Kq

was about 2.98×10^{12} $L\cdot mol^{-1}\cdot s^{-1}$ ($>10^{10}$ $L\cdot mol^{-1}\cdot s^{-1}$), indicating that static quenching occurred. In addition, the UV-visible absorption spectra of NOR were measured to investigate the existence of internal filtering effect (IFE). It was found that the UV-visible absorption spectrum of NOR had a wide absorption peak in the range of 300-370 nm. When the excitation light source was about 370 nm, the excitation spectrum of $COF_{BMTH-HB}$ and the UV-vis absorption spectrum of NOR partially overlapped (Fig. S11c), indicating that IFE might occur during the quenching process. Similarly, the excitation spectra of $COF_{BMTH-TB}$ and $COF_{BMTH-TBT}$ overlapped slightly with the UV-visible absorption spectra of NOR, but the emission intensity of 520 nm and 564 nm remained basically unchanged due to the increase of baseline (Fig. S11d,e).

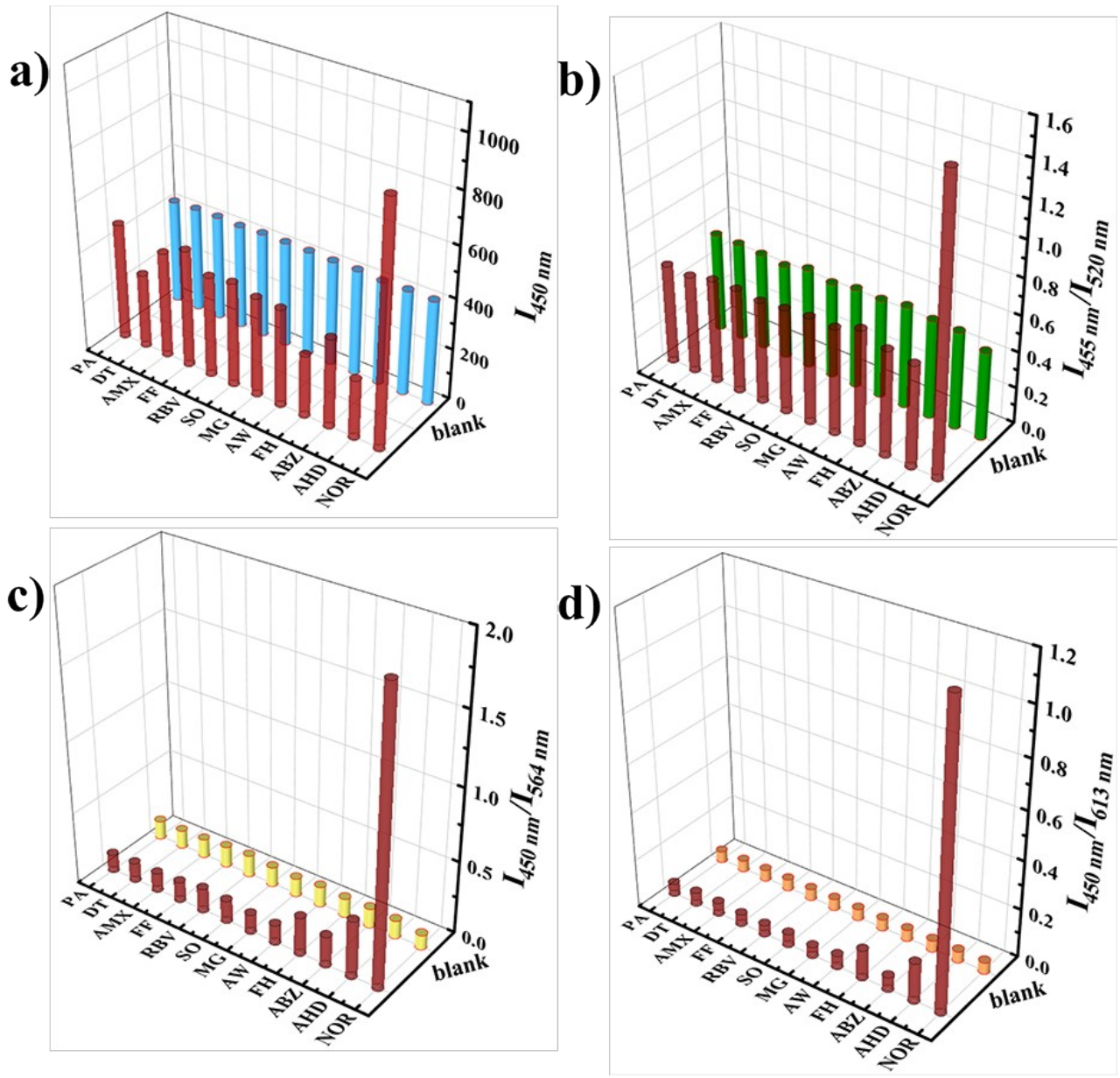

Fig. S12. Detection of common interfering chemicals by using (a) $COF_{BMTH\text{-}TFB}$, (b) $COF_{BMTH\text{-}TB}$, (c) $COF_{BMTH\text{-}TBT}$ and (d) $COF_{BMTH\text{-}HB}$.

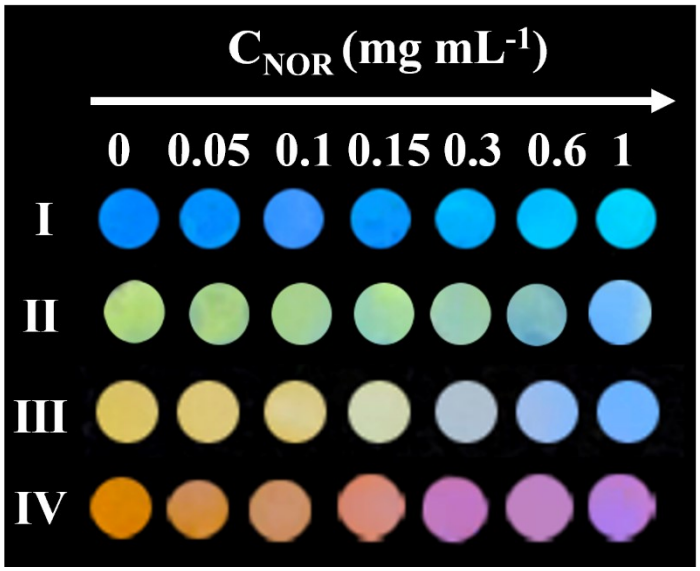

Fig. S13. Photographs of test strips of I) $COF_{BMTH\text{-}TFB}$, II) $COF_{BMTH\text{-}TB}$, III) $COF_{BMTH\text{-}TBT}$ and IV) $COF_{BMTH\text{-}HB}$ after the addition of 4 μL of NOR solution with different concentrations (from left to right: 0, 0.05, 0.1, 0.15, 0.3, 0.6 and 1 mg mL^{-1}).

Table S1. Specific surface area and pore size of hydrazone-linked COFs.

Name	BET Specific surface area / m^2 g^{-1}	pore size / nm
$COF_{BMTH\text{-}TFB}$	114.783	1.54
$COF_{BMTH\text{-}TB}$	39.806	1.54
$COF_{BMTH\text{-}TBT}$	254.784	1.61
$COF_{BMTH\text{-}HB}$	305.212	1.61

Table S2. Crystallographic parameters of hydrazone-linked COFs.

Name	Cell parameters	Interlayer	Pore size /
$COF_{BMTH\text{-}TFB}$	a = b = 30.13 Å，c = 4.10 Å	4.10	1.59
$COF_{BMTH\text{-}TB}$	a = b = 31.19 Å，c =3.83 Å	3.83	1.76
$COF_{BMTH\text{-}TBT}$	a = b = 31.15 Å，c =3.81Å	3.81	1.72
$COF_{BMTH\text{-}HB}$	a = b = 30.13 Å，c =3.89 Å	3.89	1.64

Table S3. Optical parameters of hydrazone-linked COFs.

Name	excitation wavelength /nm	emission wavelength /nm	CIE chromaticity coordinates	ΔE_g /eV	fluorescence lifetime /ns	quantum yield /%
$COF_{BMTH\text{-}TFB}$	370	450	（0.17，	3.40	3.02	1.54
$COF_{BMTH\text{-}TB}$	370	520	（0.29，	3.20	1.48	1.20
$COF_{BMTH\text{-}TBT}$	370	564	（0.41，	2.57	0.77	0.20
$COF_{BMTH\text{-}HB}$	370	613	（0.53，	2.41	0.93	0.62

Table S4. Comparison of the performance of this work with other fluorescent probes for NOR detection.

Materials	Detection limit (μg mL^{-1})	Linear range (μg mL^{-1})	Ref.
{Zn(bib)·(SO_4)·(H_2O)}n	2.2	-	1
[$Eu_2L_{0.5}(IPA)_3$]n	0.25	0.75-12.76	2
g-CDs@UiO-66	0.026	0.319-2.55	3
[Co(L)(HIPA)·H_2O]n	0.13	0.39-7	4
BUC-88	0.17	0.51-6.4	5
$COF_{BMTH-TFB}$	0.078	0.234-33	This work
$COF_{BMTH-TB}$	0.061	0.183-24	This work
$COF_{BMTH-TBT}$	0.055	0.165-36	This work
$COF_{BMTH-HB}$	0.051	0.153-48	This work

Table S5. Sensor performance parameter.

Name	Linear range	Detection limit
$COF_{BMTH\text{-}TFB}$ solution	234 ng mL^{-1}-33 μg mL^{-1}	78 ng mL^{-1}
$COF_{BMTH\text{-}TB}$ solution	183 ng mL^{-1}-24 μg mL^{-1}	61 ng mL^{-1}
$COF_{BMTH\text{-}TBT}$ solution	165 ng mL^{-1}-36 μg mL^{-1}	55 ng mL^{-1}
$COF_{BMTH\text{-}HB}$ solution	153 ng mL^{-1}-48 μg mL^{-1}	51 ng mL^{-1}
$COF_{BMTH\text{-}TFB}$ test paper	15.9 μg mL^{-1}-0.3 mg mL^{-1}	5.3 μg mL^{-1}
$COF_{BMTH\text{-}TB}$ test paper	30 μg mL^{-1}-0.3 mg mL^{-1}	10 μg mL^{-1}
$COF_{BMTH\text{-}TBT}$ test paper	11.1 μg mL^{-1}-0.3 mg mL^{-1}	3.7 μg mL^{-1}
$COF_{BMTH\text{-}HB}$ test paper	17.3 μg mL^{-1}-0.3 mg mL^{-1}	5.7 μg mL^{-1}

References

[1] Z. Lai, X. Yang, L. Qin, J. An, Z. Wang, X. Sun and M. Zhang, *J Solid State Chem*, 2021, **300**, 122278.

[2] D. Yang, Y. Shi, T. Xiao, Y. Fang and X. Zheng, *Inorg. Chem.*, 2023, **62**, 6084–6091.

[3] S. Wu, C. Chen, J. Chen, W. Li, M. Sun, J. Zhuang, J. Lin, Y. Liu, H. Xu, M. Zheng, X. Zhang, B. Lei and H. Zhang, *J Mater Chem C*, 2022, **10**, 15508-15515.

[4] Y. Wu, R. Wang, G. Dong and L. Fu, *J Solid State Chem*, 2022, **310**, 123022.

[5] C. Wang, C. Wang, X. Zhang, X. Ren, B. Yu, P. Wang, Z. Zhao and H. Fu, *Chin. Chem. Lett.*, 2022, **33**, 1353-1357.